THE ASTROPHYSICAL JOURNAL, 315:654–665, 1987 April 15

ON THE CONTRIBUTION OF INTERSTELLAR EXTINCTION TO THE 10 MICRON DUST FEATURE IN OH/IR STARS

KEVIN VOLK AND SUN KWOK
Department of Physics, The University of Calgary
Received 1986 April 18; accepted 1986 October 6

ABSTRACT

The *IRAS* Low Resolution Spectra of 467 sources with the 10 μm dust feature are analyzed. The strengths of the dust feature are determined by the ratio of the flux at 9.7 μm to the fitted continuum level. Color temperatures are derived from the fluxes of the four *IRAS* photometric bands after correcting for the effect of the 10 μm feature on the fluxes of the 12 μm band. A definite correlation between the strength of the feature and the color temperature of the continuum is found, implying that the 10 μm dust feature is largely circumstellar in origin.

A reexamination of the strength of the silicate feature for seven of the OH/IR stars used by Gehrz and colleagues in 1985 has failed to reproduce the optical depth–distance relationship found by these authors. We conclude that interstellar extinction does not play a major role in the formation of the 10 μm absorption feature.

Subject headings: infrared: sources — interstellar: grains — stars: circumstellar shells

I. INTRODUCTION

The 10 μm infrared excess in late-type stars was discovered and identified as emission from silicate dust in the circumstellar envelopes by Woolf and Ney (1969). Spectrophotometric observations show that the dust feature peaks at $\sim$9.7 μm and is commonly present in oxygen-rich stars with spectral types later than M3 (Merrill and Stein 1976*a*). Studies of sources dicovered in the IRC and AFGL surveys show that this feature often appears in absorption for infrared sources which do not have optical counterparts (Merrill and Stein 1976*b*, *c*). The change of the silicate feature from emission to absorption suggests an increasing optical depth of the circumstellar envelope, and this has been interpreted as increasing rates of mass loss as the star ascends the asymptotic giant branch (AGB). For stars with very deep absorption features, it is estimated the mass-loss rate from the star must exceed 10^{-5} $M_{\odot}$ yr^{-1} (Werner *et al.* 1980). Such high mass-loss rates should have significant implications on the advanced AGB evolution.

It has recently been suggested that the 10 μm silicate feature, rather than being circumstellar in origin, is strongly affected by contribution from interstellar extinction. Gehrz *et al.* (1985) have obtained infrared spectra of a number of OH/IR stars discovered in OH surveys and found a correlation between the depth of the silicate feature with kinematic distance. This implies that the absorption feature is mostly produced in the interstellar medium and the interstellar extinction coefficient A_v should have a value of 4–6 mag per kpc, or 2–3 times the commonly accepted value. This difference is attributed to the OH/IR stars being selected on the basis of their radio data rather than due to visual wavelength observations. It is argued that the traditional determination of A_v is probably biased toward regions of low A_v because this is usually done by choosing luminous stars of sufficiently low visual magnitude that very accurate photometric colors can be determined, thus selecting those areas of the sky with small amounts of interstellar extinction. If these arguments are correct, then the mass-loss rates of OH/IR stars must have been overestimated in the past and their importance on evolution greatly exaggerated.

A similar study of 20 unidentified OH/IR stars was carried out by Herman *et al.* (1984). But instead of using the kinematic distances, these authors derive the distances from the phase-lag radii and the angular extent of the OH emission. Contrary to the conclusion of Gehrz *et al.* (1985), no significant correlation between the strength of the silicate feature and the distance is found.

An alternative method to determine the influence of interstellar extinction on the 10 μm feature is to seek a correlation between the color temperature of the stellar continuum and the strength of the silicate feature. This method has been used by Evans and Beckwith (1977) who find that the silicate feature is only in strong absorption when the color temperature is below 500 K. Since previous analyses relied on near-infrared photometry between 2 and 10 μm for color temperature determination, the results may have been affected by interstellar extinction. A similar analysis using long wavelength data could yield more definitive results.

Generally speaking, if the 10 μm feature is formed entirely in the circumstellar envelope then one would expect the underlying continuum to have a color temperature well below the dust condensation temperature because the optical depth at 10 μm must be greater than unity. Furthermore, a deep self-absorption feature should correlate with a low color temperature of the continuum as the absorbed flux is redistributed into the far-infrared. However, in order to obtain a statistically meaningful result a much larger observational sample is needed.

The Low Resolution Spectrometer (LRS) on the *Infrared Astronomical Satellite* (*IRAS*) has a resolving power of $\lambda/\Delta\lambda \approx 40$ in the wavelength band from 7.8 to 22 μm. During the *IRAS* all-sky survey, a large number of stars with the 10 μm dust feature were detected by the LRS, and many of these objects are likely to be OH/IR stars. A large unbiased observational data base therefore now exists for a detailed

[1] Publication of the Rothney Astrophysical Observatory, No. 40.

study of this problem. In this paper, we have (1) selected a group of stars with the 10 μm feature in emission or absorption; (2) determined the strength of the dust feature by performing a fit to the continuum; (3) corrected for the fluxes of the 12 μm photometric band by using the fluxes of the calculated continuum; and (4) derived color temperatures of the continuum using the fluxes of the four photometric bands. The results of operations (2) and (4) are compared to determine whether a correlation is present and conclusions are drawn on the circumstellar or interstellar origin of the dust feature.

II. THE DATA BASE

The *IRAS* Low Resolution Spectra Catalog (LRSC) contains 5449 sources, of which most are identified as late-type stars. The stellar sources are classified by a two-digit number according to the presence of the 10 μm feature in emission or absorption and the slope of the underlying continuum (*IRAS Explanatory Supplement* 1985):

1. *LRSC class 10–19.*—2246 objects with no spectral features which are identified with stars of spectral type M5 or earlier.

2. *LRSC class 20–29.*—1738 objects which show the 10 μm feature in emission and which have a "blue" continuum, identified with M stars with dust envelopes.

3. *LRSC class 30–39.*—230 objects which show the 10 μm feature in absorption and which have a "blue" continuum, identified with M stars with thicker dust envelopes.

4. *LRSC class 60–69.*—78 objects which show the 10 μm feature in emission and which have a "red" continuum, identified with M stars with a still thicker dust envelope.

5. *LRSC class 70–79.*—67 objects which show the 10 μm feature in absorption and which have a "red" continuum, identified with M stars with the thickest dust envelopes of all the stars with the 10 μm feature in their spectrum.

The "red" continuum versus "blue" continuum classification is based upon the spectral index between 15 and 22 μm. If the λF_λ value rises between 22 and 15 μm the spectrum defined as "blue," otherwise "red". Figure 1 shows examples of the LRS spectra with the 10 μm feature from LRSC classes 21–39.

The above classification scheme suggests a continuous evolution from class 20's to class 30's and then on to class 70's as the optical depth of the dust feature increases and the temperature of the optically thick surface (continuum) declines. It is not clear how the class 60 objects fit into this evolution, as they imply a comparatively low optical depth judging by the feature but a low temperature of the dust emission region on the basis of the continuum. Comparison of the LRSC spectra

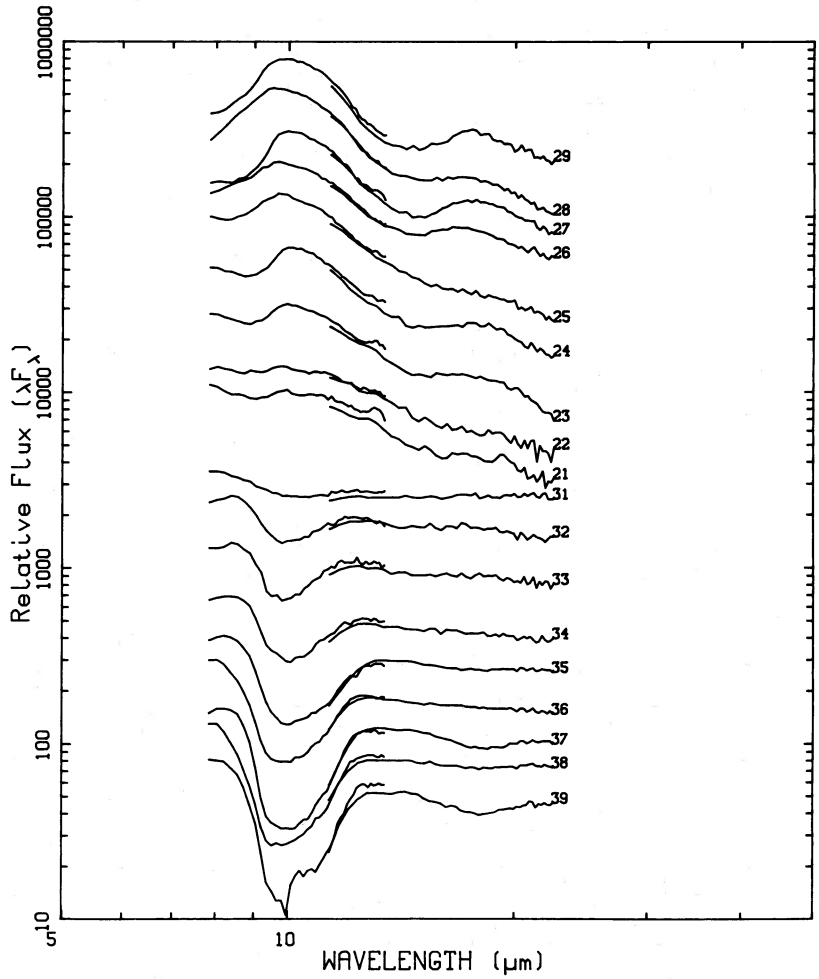

FIG. 1.—Examples of LRS spectra for objects with the 10 μm silicate feature in emission and absorption. Each spectrum is labeled with its LRSC classification number.

with model radiative transfer calculations suggests that some of the class 60 objects are in a state of post–AGB evolution after the mass-loss process has stopped (Volk and Kwok 1987).

The four LRSC classes with the 10 μm feature are further divided into subclasses from 1 to 9 based on the strength of the 10 μm feature. For the emission feature objects,

$$N = 10[[\ln [F_\lambda(9.8\ \mu\text{m})] - \{0.589 \ln [F_\lambda(7.9\ \mu\text{m})] + 0.411 \ln (F_\lambda(13.3\ \mu\text{m}]\}]] \quad (1)$$

gives the spectral subclass when rounded to the nearest single digit integer. For the absorption objects this formula is changed only in the replacing of the constant 10 by -5. The F_λ values are obtained by averaging flux values over 0.25 μm either way from the nominal wavelength. It appears that the numerical coefficients 0.589 and 0.411 in equation (1) were obtained by assuming the continuum to have a λ^{-4} spectral shape, although this is not explicitly stated in the *IRAS Explanatory Supplement* (1985).

Among the 2113 objects in the LRSC that show a dust feature at 10 μm, 467 are found to have good photometric fluxes in all four of the *IRAS* bands. These 467 objects break down into 363 class 20's, 38 class 30's, 14 class 60's, and 40 class 70's. These 467 objects constitute the data base from which this study is based.

At this point, we are already able to draw some qualitative conclusions on the effects of interstellar absorption. There are 2246 stars in the class 10's but only 230 stars in class 30's, 150 of which are in class 31 or 32. Since stars with no circumstellar dust (generally with spectral types earlier than M3) will also suffer from interstellar extinction and are therefore expected to show the 10 μm absorption feature, the large number of featureless class 10's objects (many of which are in the Galactic plane) compared to small number of class 30's suggests that interstellar absorption is not a dominant factor in creating the 10 μm feature.

III. THE METHOD

Our objective is to obtain the strengths of the 10 μm feature and the color temperatures for the 467 objects. A positive correlation between the two then implies that the 10 μm feature is largely circumstellar in origin.

The color temperature of the continuum is determined from the four *IRAS* photometric bands. First, it is necessary to correct the 12 μm flux value for the effect of the 10 μm feature, for the feature is in many cases strong enough to significantly affect the photometry. A power law of the form

$$F_\lambda \propto \lambda^\beta \quad (2)$$

is fitted to the continuum on either side of the feature, at 7.9 and 15.5 μm averaged over 0.25 μm. The value of 15.5 μm is chosen on the long wavelength side rather than 13.3 μm as used in the *IRAS Explanatory Supplement* (1985) because it is found that the continuum blends more smoothly to the data at 15.5 μm than at 13.3 μm. The power-law fit is then taken to represent the true continuum over the feature. The derived values for β are often significantly different from the value of -4 expected for a Rayleigh-Jeans distribution. This is another manifestation of the low temperature of the emitting region where the spectra often peak beyond 5 μm. In some cases problems are encountered due to mismatches between the two halves of the LRSC data, for the LRS data are actually taken in two sections—7.7–13.4 μm and 11.0–22.6 μm—and the two sections sometimes do not match well in the overlapping region. This is a problem in a small number of cases, although the class 70's turns out to have a higher incidence of such problems than the other groups. As a result a greater weight should be given to the class 20's and 30's.

Assuming that the fit accurately reflects the continuum, the flux of the 12 μm band can be corrected by a factor R given by

$$R = \frac{\int F_{\lambda,c}\, r(\lambda) d\lambda}{\int F_\lambda\, r(\lambda) d\lambda}, \quad (3)$$

where $F_{\lambda,c}$ is the continuum flux fit function and $r(\lambda)$ is the filter response function as given in the *IRAS Explanatory Supplement* (1985). This correction factor, rather than the absolute values of $F_{\lambda,c}$, is used to derive a 12 μm flux value because the sources may be variable. The values for R are considerably different from 1 in some cases, particularly for class 29 objects.

Typical spectra of sources with the dust feature in emission and absorption, together with the continuum fit, are presented in Figures 2 and 3. In the case of the emission object (class 29) there is a additional dust emission feature at 20 μm (also due to silicates), so the actual continuum is likely to lie slightly below the dotted line. This should not seriously affect our results, however. The class 30's do not show the 20 μm feature and the power-law fit runs smoothly into the continuum. This weakness of the 20 μm feature in stars with the 10 μm feature in absorption is also confirmed by theoretical radiative transfer model calculations (Volk and Kwok 1987).

The color temperature T of the sources are obtained by performing a least-squares fit to the four photometric band fluxes using the Planck function. The quantity to be minimized can be defined as

$$\chi^2 = \sum_{i=1}^{4} \{\log (\lambda F_\lambda)_i - \log [\lambda_i B_\lambda(T)]\}^2, \quad (4)$$

where

$$B_\lambda(T) = A\lambda^{-5}[\exp (hc/\lambda kT) - 1]^{-1}. \quad (5)$$

The parameters to be found are A and T. Setting the partial derivative of χ^2 with respect to A equal to zero gives A directly, while the partial derivative with respect to T yields a nonlinear equation which can be solved for T using the Newton's method. The derived values for T are listed in Table 1.

III. RESULTS

We are able to fit all but two of the 467 objects satisfactorily. The average temperatures ($\langle T \rangle$) for classes 20–24, 25–29, 30–39, 60–69, and 70–79 are presented in Table 2 along with the standard deviations in the mean (σ) and the maximum ($T_{\max}$) and minimum ($T_{\min}$) values. We should note that the lower class 20's are expected to be of two populations: sources with very low dust optical depth and those of optical depth near unity for which the feature is in the process of becoming an absorption feature. Since these two groups of objects with very different optical depths can have similar feature strengths, a spread of T for this class is therefore not unexpected.

With the exception of three stars with $T \approx 2500$ K, the maximum temperature in the sample is $\sim$1700 K, well below the expected photospheric temperatures of stars. This suggests that the dust condensation temperature is $\sim$1700 K. The maximum temperature of the absorption objects is 660 K, suggesting that the silicate feature is in self-absorption against an optically thick dust continuum. There is no evidence of any hot stellar temperature object with a 10 μm absorption feature.

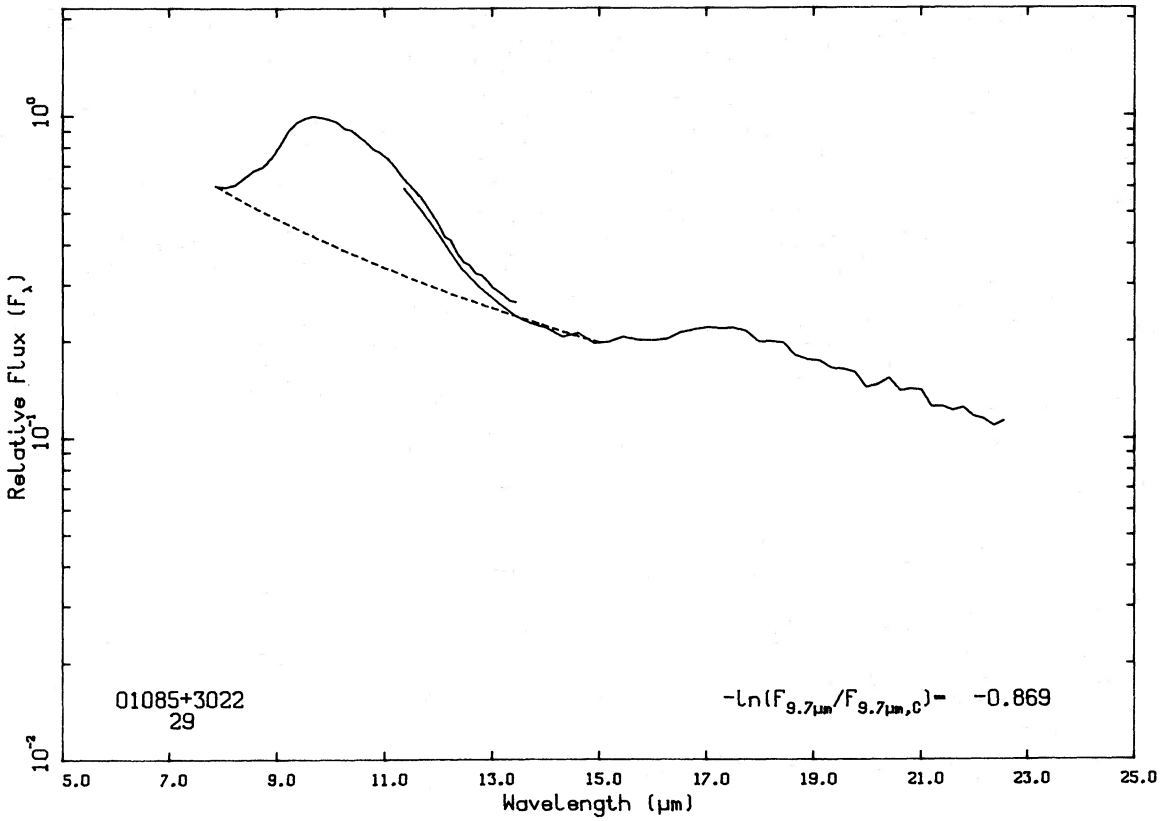

FIG. 2.—The LRS spectra for a class 29 object. The fitted continuum is shown by the dashed line.

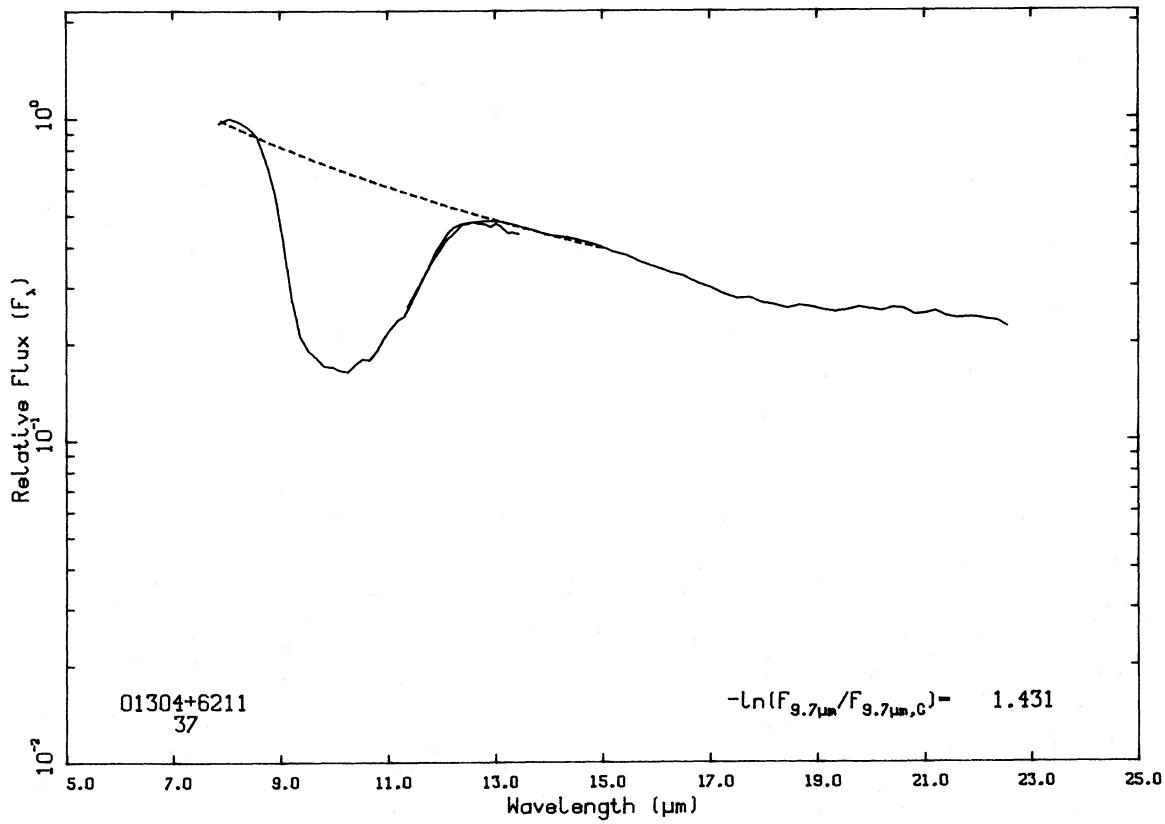

FIG. 3.—The LRS spectra for a class 37 object. The fitted continuum is shown by the dashed line.

TABLE 1

COLOR TEMPERATURE AND 10 MICRON FEATURE STRENGTH FOR 467 *IRAS* SOURCES

IRAS Name	LRSC	S	T(K)	IRAS Name	LRSC	S	T(K)	IRAS Name	LRSC	S	T(K)
00007+5524	22	-2.4	990	04525+3028	69	-6.9	138	07027-7934	73	3.4	254
00042+4248	26	-5.7	702	04566+5606	27	-7.9	627	07034-3551	21	-2.8	743
00087+5833	63	-2.8	139	04575+1251	27	-6.5	975	07051+6601	29	-9.1	1252
00172+4425	24	-2.2	575	05052-8420	27	-7.7	637	07080-1610	22	-1.3	468
00193-4033	28	-8.1	2609	05073+5248	24	-3.5	342	07080-5948	28	-7.4	956
00428+6854	27	-6.3	393	05096-4834	25	-5.9	650	07118-3438	29	-8.3	823
00479+4614	29	-9.4	396	05098-6422	26	-5.7	426	07152-3444	29	-9.2	662
01085+3022	29	-8.7	1188	05151+6312	29	-9.3	1558	07180-1314	25	-4.5	449
01133+2530	22	-0.5	527	05176-1755	22	-3.0	752	07209-2540	24	-3.3	1037
01144+6658	21	-1.3	308	05208-2035	29	-5.7	281	07232-0544	23	-4.5	391
01159+7220	22	-2.4	698	05345+3157	31	1.5	108	07245+4605	23	-2.5	605
01304+6211	37	14.4	328	05354+2458	22	-3.2	455	07284-0940	26	-5.0	339
01438+1850	23	-3.3	609	05358-0704	71	1.8	158	07304-2032	29	-8.9	406
01556+4511	22	-3.2	690	05361+4644	23	-2.8	321	07308+3037	27	-7.1	2420
02000+0726	22	-2.1	468	05367+3736	25	-5.7	607	07329-2352	27	-7.1	381
02143+4404	22	-2.4	724	05388+3200	23	-3.4	611	07358-3243	75	2.0	107
02145+7831	26	-5.7	456	05404-2343	22	-2.6	788	07399-1435	79	16.2	126
02188+5652	26	-6.5	591	05411+6957	29	-9.1	739	07418-2850	24	-3.7	638
02192+5821	26	-7.6	1035	05528+2010	26	-6.8	872	07434-3750	22	-1.9	828
02234-0024	29	-7.3	394	05533+3022	22	-1.7	315	07446-3210	27	-7.3	339
02302+4525	24	-4.8	543	05534+4530	25	-5.9	770	07536-2830	28	-7.9	367
02345+5422	23	-2.2	483	05543+5002	29	-7.3	335	07556-2017	29	-9.5	903
02351-2711	29	-9.7	1660	05559+3825	27	-6.4	619	07559-5859	22	-1.8	193
02384+3418	23	-3.0	718	05559+7430	24	-4.4	656	07585-1242	25	-5.6	757
02401-0013	32	1.8	137	06012+0726	22	-1.8	485	08002-3803	27	-5.2	285
02407+3602	29	-8.5	1066	06027-1628	25	-4.2	634	08003+3629	23	-2.7	645
02427-5430	22	-3.7	1002	06036-2411	26	-7.0	833	08074-3615	22	-1.7	688
02455-1240	25	-3.9	1246	06038-0541	25	-4.6	436	08124-4133	27	-7.1	908
02469+5646	28	-8.4	671	06053-0622	76	12.6	114	08171-2134	22	-2.1	386
02522-5005	24	-5.0	664	06073+1249	74	4.6	107	08182-6000	32	1.8	322
03074-8732	27	-6.5	388	06084-0611	75	8.6	96	08189+0507	21	-1.7	862
03082+1436	21	-1.6	1006	06092+2255	23	-3.9	463	08196+1509	24	-3.6	828
03170+3150	25	-5.3	441	06139+3313	22	-3.1	632	08200-2528	24	-4.6	1199
03206+6521	34	6.1	362	06140-2729	23	-3.4	824	08211-3302	29	-9.6	384
03236+5836	73	2.4	130	06193-0349	27	-6.7	696	08220-0821	29	-9.6	1139
03287-1535	29	-9.4	363	06210+4918	21	-1.1	569	08247-4223	33	5.2	107
03293+6010	33	4.8	355	06216-0004	27	-7.3	411	08260-7054	24	-3.7	350
03313+6058	22	-1.8	251	06250+6134	23	-2.4	407	08299-3148	26	-4.1	431
03336-7636	26	-5.6	718	06255-4928	29	-8.9	1561	08349-5945	21	-1.2	699
03482-5213	22	-2.5	1097	06259-1301	24	-3.8	1276	08357-1013	25	-4.1	1126
03507+1115	26	-5.7	814	06278+2729	27	-6.9	794	08363-4643	22	-1.8	399
04000+5052	78	3.6	104	06297+4045	27	-6.4	566	08372-0924	24	-3.7	966
04020-1551	22	-2.8	1035	06300+6058	28	-8.5	382	08375-1707	22	-2.5	770
04094-2515	24	-4.6	904	06310-6650	25	-4.5	1072	08380-1438	27	-6.4	852
04140-8158	24	-5.3	760	06319-0501	32	3.0	269	08470-4321	36	8.2	134
04166+4056	23	-3.8	859	06363+5954	27	-7.6	770	08500-3254	27	-6.3	250
04188+2819	69	-5.2	180	06391-2213	23	-1.5	332	08502-4606	27	-5.0	168
04255+1003	21	-2.2	703	06403-1424	23	-2.8	380	08534-1901	23	-3.0	480
04265+5718	22	-2.3	448	06434-3628	23	-3.1	518	08538+2002	23	-1.6	868
04382-1417	21	-2.1	653	06491-0654	24	-2.9	477	09069+2527	23	-2.7	673
04387-3819	23	-3.7	1168	06496-1858	26	-5.3	464	09072-5933	26	-5.5	380
04395+3601	62	-1.7	182	06534-1647	22	-2.9	383	09076+3110	22	-2.9	1169
04396+0647	22	-3.3	472	06582+1048	28	-6.7	520	09199-5447	79	7.4	126
04404-7427	29	-8.4	1334	06582+1507	22	-2.3	306	09213-5723	22	-2.4	439
04483+2826	22	-1.3	327	07013-1128	31	1.8	159	09235-2347	28	-8.2	613

TABLE 1—*Continued*

IRAS Name	LRSC	S	T(K)	IRAS Name	LRSC	S	T(K)	IRAS Name	LRSC	S	T(K)
09256-6324	22	-1.2	287	14371+3245	22	-2.7	772	17150-3224	74	4.6	160
09425+3444	24	-4.5	1121	14390+3147	23	-2.6	512	17189-6501	24	-3.1	417
09429-2148	28	-7.4	1385	14394-6004	79	14.0	98	17211-3537	35	4.2	107
09508-4345	22	-2.6	632	14425-6023	35	4.0	116	17222-5038	25	-2.6	266
09578-5649	72	4.8	97	14473-6842	29	-6.4	418	17230+0113	29	-9.3	449
10019-5712	77	4.0	101	14531-5337	27	-6.6	413	17255-5355	25	-3.5	324
10028-5825	64	-3.4	162	14550-1214	22	-1.9	728	17256+0504	26	-4.6	340
10056-5300	29	-13.1	675	14591-4438	26	-5.6	1680	17265-0725	22	-3.0	673
10091-7049	22	-3.0	759	14595-4124	29	-7.1	322	17319-6234	31	2.2	361
10133-6758	23	-2.2	289	14598-7124	22	-2.8	514	17329+5359	25	-4.6	458
10133-5413	22	-2.6	545	15060+0947	28	-6.7	1333	17334+1537	29	-8.4	836
10171-6205	24	-2.5	258	15100-5613	75	9.6	93	17361+5746	28	-7.9	1170
10189-3432	28	-7.8	634	15193+1429	22	-2.4	352	17462-8647	22	-1.7	563
10215-5916	66	-4.0	168	15193+3132	24	-4.6	1194	17484-0800	29	-8.7	906
10320-5928	71	3.2	104	15223-0203	24	-4.4	1127	17534-3030	21	-0.9	277
10323-4611	24	-3.5	682	15246-5612	73	5.8	105	17534+2603	23	-2.8	429
10329-3918	21	-0.5	336	15254-7718	27	-5.7	368	17554+2946	26	-5.3	355
10394-5747	26	-6.7	246	15255+1944	29	-10.0	658	17579+2335	29	-8.7	916
10403-7612	25	-4.9	436	15262+0400	27	-6.1	1558	18050-2213	26	-6.2	922
10411+6902	23	-3.6	739	15278-5620	76	9.4	98	18069+0911	28	-6.2	573
10456-5712	23	-2.9	402	15314+7847	21	-1.7	2353	18076+3445	27	-5.8	387
10521+7208	26	-5.7	420	15332-6430	26	-5.6	375	18095+2704	69	-9.0	540
10580-1803	22	-3.1	709	15341+1515	22	-1.8	740	18112+1227	25	-5.0	461
11000-6153	23	-2.9	175	15356-6722	27	-5.9	1133	18125+3010	23	-3.6	501
11023-5231	27	-4.7	260	15410-0133	21	-1.8	1316	18125-7741	23	-3.3	606
11081-4203	25	-4.3	480	15423-6534	23	-3.2	447	18162-2048	74	3.6	94
11125+7524	23	-3.9	625	15471-5644	21	-1.4	347	18183+0554	27	-6.1	256
11287-6918	24	-3.9	435	15483+1517	24	-4.1	1151	18186+3143	22	-2.7	650
11296-4431	24	-2.8	696	15530-5231	75	9.0	101	18261-1748	21	-2.0	288
11438-6330	38	14.0	325	15566+3609	26	-5.8	809	18276+8236	28	-7.9	1136
11452-4553	22	-2.7	498	15576-1212	29	-7.7	400	18280-5639	22	-3.0	832
11482-4718	27	-4.9	333	15589-2850	29	-9.8	419	18281+2149	25	-4.0	249
11485-4849	29	-6.7	438	16011+4722	24	-4.6	592	18298-2111	34	6.4	247
11516-6201	39	13.2	211	16029-3041	32	4.6	290	18302-1052	74	4.2	139
11525-5057	29	-8.3	1167	16057-6533	25	-4.0	267	18309-6955	24	-4.7	665
11575-7754	25	-3.2	220	16081+2511	23	-3.5	887	18316-0602	79	15.6	108
12151-4610	26	-6.1	889	16105-4205	35	9.8	318	18324-1751	28	-4.9	229
12222-4652	22	-2.7	373	16219-5048	27	-7.0	240	18349+1023	26	-6.7	545
12233-5920	29	-9.8	379	16235+1900	23	-3.7	1313	18394+2845	25	-4.1	364
12379-4959	29	-8.5	351	16260+3454	28	-7.3	373	18413+1354	29	-8.2	1475
12384-4536	24	-3.6	1273	16263-5533	33	5.0	364	18436+4334	27	-6.4	385
12405-6238	79	8.0	97	16367-4701	71	1.6	118	18460+1903	22	-2.5	286
12496-7650	33	4.0	163	16418+5459	24	-4.3	609	18467-4802	22	-1.1	673
13001+0527	21	-2.0	692	16460-4022	36	11.4	340	18501-2132	23	-3.2	523
13170-5404	23	-3.1	443	16473+5753	22	-1.5	1158	18549+0208	39	3.8	148
13368-4941	22	-2.3	686	16482-2039	29	-5.5	261	18560-2954	27	-7.1	811
13466-3512	65	-4.0	336	16494-1252	22	-2.6	511	18566+0408	79	13.4	110
13479-5436	27	-6.6	1133	16559-2557	29	-8.9	392	18595-3947	26	-6.0	799
14003-7633	22	-2.3	1007	16571-7548	27	-6.3	633	19007-3826	24	-4.4	385
14020-3515	29	-9.6	882	16594-4656	74	6.0	190	19026-2528	22	-1.6	262
14030-4629	28	-6.8	360	17001-2029	28	-6.9	354	19032-4602	29	-12.0	636
14083-5649	67	-4.0	204	17074-4549	79	12.2	99	19039-4839	22	-2.1	491
14086-2839	26	-6.3	1257	17079-7405	21	-1.9	545	19042-4858	29	-9.3	1572
14086-6907	27	-6.1	1115	17080-3215	28	-9.2	408	19059-2219	28	-7.8	1236
14106-2940	29	-7.9	1066	17088-4221	39	13.0	233	19089+1542	62	-0.9	186
14117-5357	26	-5.6	349	17102-1031	27	-7.2	798	19093-3256	28	-8.2	1332
14142-1612	22	-2.4	632	17103-0559	28	-7.6	1439	19095+0930	75	4.6	84
14206-6151	72	2.0	96	17119+0859	28	-8.5	662	19098+6601	22	-1.4	584
14247+0454	24	-4.7	974	17121-5747	28	-6.5	353	19098-1502	27	-6.2	730
14319-7154	29	-7.3	283	17131-6225	29	-7.7	371	19126-0708	22	-2.3	992

TABLE 1—*Continued*

IRAS Name	LRSC	S	T(K)	IRAS Name	LRSC	S	T(K)	IRAS Name	LRSC	S	T(K)
19157-1706	28	-7.4	1373	20144+3526	79	7.6	119	22035+3506	21	-2.3	648
19161+2343	31	1.2	366	20168-7849	29	-10.8	574	22134+5834	75	6.0	107
19167-2101	22	-1.4	378	20173+3714	35	2.6	108	22142-8454	23	-2.9	751
19178-2620	26	-5.2	343	20180+3558	36	5.2	106	22176+6303	76	10.0	111
19188-1603	23	-3.3	1210	20234-1357	27	-6.2	442	22177+5936	38	14.0	276
19192+0922	31	2.6	660	20248+7505	23	-3.8	1171	22187+5559	72	3.2	102
19193+1504	79	6.4	100	20267+2105	24	-3.5	292	22190-0751	25	-4.9	515
19207+1410	72	3.6	101	20272+3535	39	12.2	166	22212+5542	26	-6.7	269
19219+0947	69	-9.4	165	20278+3521	75	3.2	108	22230-4841	22	-2.7	907
19231+3555	29	-9.0	1141	20359-3806	21	-1.8	723	22231-4529	29	-9.0	772
19231-2717	22	-2.3	239	20365+1154	24	-3.8	1090	22233+3013	29	-11.0	1619
19232+5008	26	-6.5	-	20392+1141	23	-3.0	1048	22272+5435	72	1.2	194
19233+7627	23	-2.4	503	20431+1754	23	-3.0	807	22282+5644	28	-7.8	325
19238-3521	22	-2.3	452	20438-0415	22	-2.0	1494	22512+6100	28	-8.6	300
19240+3615	29	-7.9	623	20440-0105	27	-7.4	1642	22516+0838	29	-8.5	778
19247-1722	23	-3.2	480	20444+0540	29	-7.3	309	22525-2952	22	-2.8	933
19250-6953	22	-1.7	428	20454+1908	22	-2.0	434	22540-5740	22	-2.3	703
19296+4331	25	-6.2	581	20467-0044	21	-1.5	850	23017+6007	34	3.2	110
19354+5005	22	-1.8	479	20479+0554	23	-3.5	531	23041+1016	22	-2.4	1049
19356+1136	24	-4.0	425	20484-7202	29	-8.2	607	23107-6833	23	-2.9	323
19361-1658	29	-9.2	-	20526-5431	22	-2.3	655	23151+5912	39	19.0	122
19412+0337	29	-9.0	512	20541-6549	29	-9.1	1140	23152+6034	72	2.0	131
19422+3506	28	-7.7	439	20547+0247	32	3.8	451	23213-4521	28	-7.8	561
19440-4118	22	-1.4	488	20549+5245	27	-6.8	263	23239+5754	67	-5.0	219
19442-0829	29	-7.6	308	21028+2711	23	-3.8	445	23284+5958	29	-10.1	340
19474-0744	28	-8.3	761	21044-1637	27	-6.9	647	23365+5159	25	-5.6	649
19495+0835	28	-6.7	1074	21069-3843	29	-10.3	1467	23416+6130	69	-9.8	281
19503+2219	24	-4.7	491	21073+5138	26	-4.7	216	23425+4338	26	-6.2	1132
19528-2919	23	-2.6	1504	21197-6956	22	-1.9	426	23496+6131	27	-6.4	1401
19548+3035	21	-1.4	293	21206-4054	29	-8.1	614	23528+4821	22	-2.6	722
19550-0201	27	-7.6	1097	21208+7737	26	-5.7	571	23541+7031	31	2.0	237
19566+3423	36	6.2	215	21270+7135	29	-8.7	643	23558+5106	24	-4.8	660
19598+3324	72	3.6	107	21286+1055	26	-6.2	450				
20000+4954	69	-8.8	462	21305+2118	26	-4.6	1034				
20015+3019	29	-9.8	312	21318+5631	21	-1.0	410				
20042-4241	28	-7.8	1112	21334+5039	79	7.0	103				
20043+2653	39	7.6	217	21368-3812	21	-1.3	473				
20046-8131	29	-7.5	1018	21381+5000	32	3.2	150				
20047+1248	28	-7.8	733	21439-0226	23	-3.7	815				
20052+0554	29	-9.3	1115	21456+6422	28	-8.3	752				
20075-6005	22	-3.8	559	21543-1421	21	-2.1	618				
20077-0625	23	-3.0	741	21554+6204	38	12.6	287				
20079-0146	21	-1.7	736	21558+5907	33	4.4	159				
20094-1121	22	-2.6	669	21563+5630	26	-5.6	389				
20135-7152	29	-8.2	1070	22017+2806	26	-7.1	1201				

TABLE 2

STATISTICS OF THE COLOR TEMPERATURE T AS A FUNCTION OF THE LRSC CLASS

LRSC Class	$\langle T \rangle$ (K)	σ (K)	T_{min} (K)	T_{max} (K)
20–24	658.6	22.5	175.0	2353.0
25–29	706.9	29.9	168.0	2609.0
30–39	240.4	18.5	106.0	660.0
60–69	240.1	27.9	138.0	540.0
70–79[a].....	117.4	4.3	84.0	254.0

[a] Class 70–79 may contain objects (e.g., H II regions) which are not AGB stars.

It is also interesting to note how small the σ value is for the class 70–79 objects in spite of the relatively small number of objects and the possible problems with the continuum for these types of objects. The mismatching problem mentioned earlier does not seem to have a major effect on the determination of the color temperature.

Since the amount of interstellar reddening is small at $\lambda > 20$ μm, our color temperature determination is therefore much more reliable than previous efforts which were based on near-infrared measurements. In order to demonstrate the effects of interstellar reddening on the derived color temperature, we have performed tests based on an interstellar extinction value of $A_v = 5$ and an extinction law of the form

λ^{-1}. The color temperature of a 2500 K blackbody derived from four measurements at 12, 25, 60, and 100 μm is reduced to 1300 K. A further 5 mag of extinction produces a temperature of 800 K. In order to create color temperatures of $\sim$450 K found for absorption objects, $A_v \approx 35$ is needed. A value of $A_v \approx 35$ requires an object at a distance of 6–9 kpc, using the large extinction coefficient of Gehrz *et al.* (1985). This is near or beyond the distance limit for an AGB star to be observed by the LRS. As most of the class 30 objects are confined to the plane and have color temperatures much less than 450 K, it is very unlikely that their low color temperatures are due to interstellar extinction.

The effect of interstellar extinction on low-temperature objects is less severe. For a 400 K object, the error on color temperature introduced by 5 mag of reddening is no more than $\sim$10%. The low color temperatures of the absorption objects are therefore most likely to be the result of flux redistribution in the circumstellar envelope rather than by reddening.

As noted earlier the β values from equation (2) are found to be significantly different than the value of 4 (cf. eq. [1]) assumed in the *IRAS Explanatory Supplement* (1985). For this reason the quantity defined by $s = 10 \ln (F_{9.7\ \mu m,\ c}/F_{9.7\ \mu m})$ found from the actual β value is a better indicator of the strength of the 10 μm feature than is the LRSC sublcass. In Figure 4 the color temperature is plotted against s for the 465 objects. We can see that the color temperature decreases as the silicate feature goes from emission to absorption, consistent with the fact that it is circumstellar in origin. The center of Figure 4 (small s and low T) is presumably populated by stars which 10 μm feature is in the process of going from emission to absorption and in fact have a large optical depth ($\tau \approx 4$).

IV. ALTERNATIVE METHOD

This study is limited to $\sim$20% of all LRSC objects with the 10 μm feature because many of these objects do not have good fluxes at all four photometric bands (often with upper limits only at 100 μm). The size of the data base would be greatly increased if the color temperature can be reliably determined for all objects. Since for individual objects the LRS fluxes are not always in agreement with the photometric fluxes, the color temperature cannot be derived by combining the fluxes from both instruments. However, the shape of the continuum can be obtained by using the LRS data alone and this is in fact represented by the value of β.

We have therefore also calculated another set of color tem-

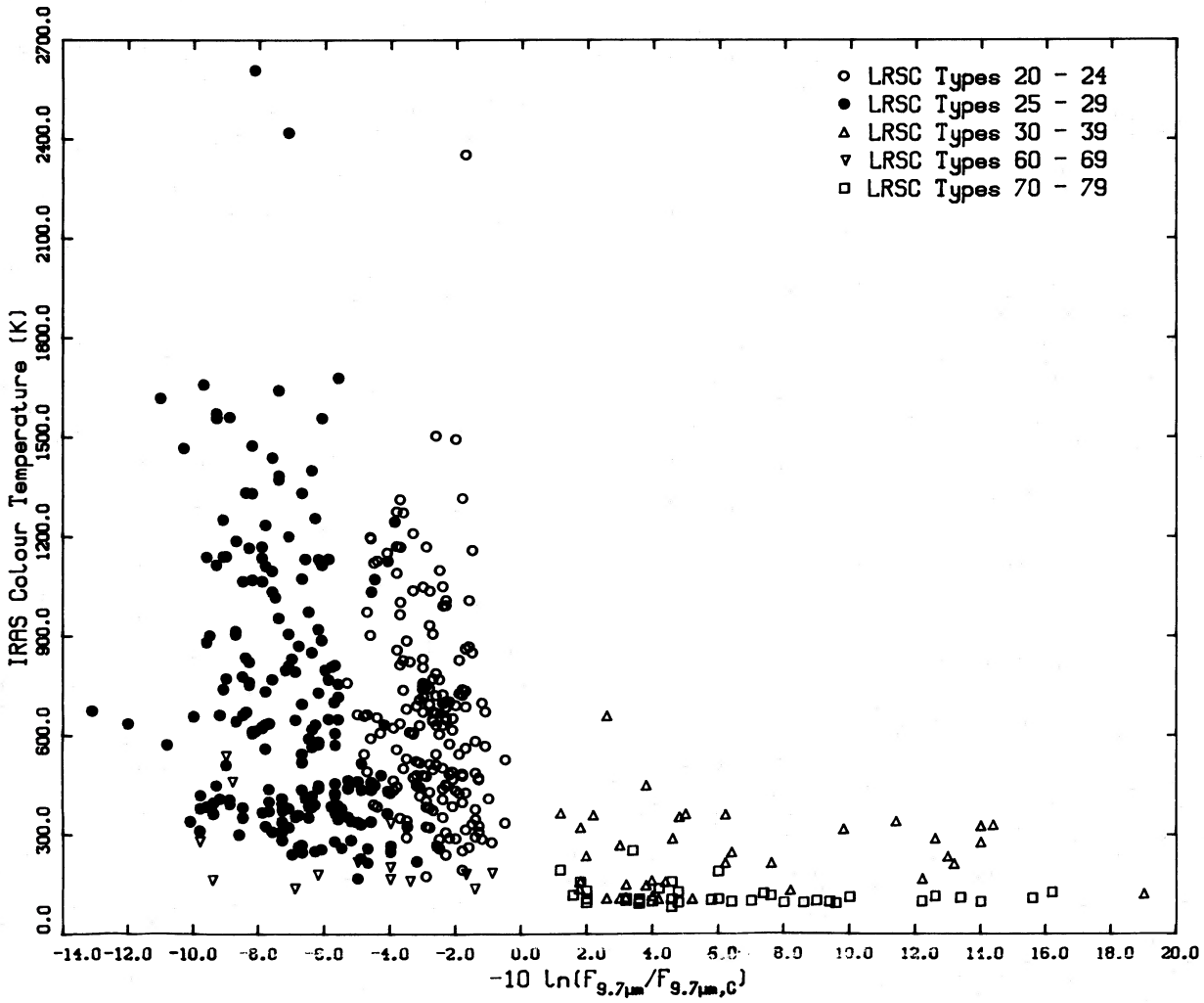

FIG. 4.—The derived color temperatures plotted against the strengths of the 10 μm feature. Different symbols represent the LRSC classification of the sources.

peratures assuming that the 7.9 and 15.5 μm flux values sample a blackbody continuum. The values for β are calculated simply from the slope of the line defined by the 7.9 and 15.5 μm flux values on a log-log plot:

$$\beta = [\log (F_{\lambda_1}) - \log (F_{\lambda_2})]/\log (\lambda_1/\lambda_2) . \quad (6)$$

Substituting the blackbody formula into equation (3) gives the expression

$$\beta = -5 + \frac{\log [\exp (a/\lambda_2) - 1] - \log [\exp (a/\lambda_1) - 1]}{\log (\lambda_1/\lambda_2)} , \quad (7)$$

where $a = hc/kT$. This procedure is less accurate than the first one because of the uncertainty about whether the continuum is actually being sampled and whether the objects behave like a blackbody over the restricted range of wavelengths under consideration here.

The color temperatures T' are calculated by interpolation of the β values against a list of $\beta(T)$ values generated from equation (4) above. The values for T' are generally similar to the values for T calculated by the first method, but there is a definite systematic effect present resulting in $T' < T$ for emission objects and $T' > T$ for the absorption objects. This is probably due to the presence of residual dust emission or absorption at 15.5 μm. Since the first method determines T over a much larger range in wavelength we therefore have to conclude that the second procedure is not as satisfactory and the color temperature for all of the 2113 objects cannot be reliably obtained.

V. THE τ-DISTANCE RELATIONSHIP

The large value of interstellar extinction found by Gehrz *et al.* (1985) is based on a correlation between the kinematic distances and the optical depths at 11.4 μm for 11 OH/IR stars with no optical counterparts. Since the LRS has better spectral resolution, values for the depth of the silicate absorption feature can be determined more accurately by the method described in this paper. A search of the LRSC showed that seven of the 11 OH/IR stars used by Gehrz *et al.* (1985) are in the LRSC and their spectra are plotted in Figure 5. All of the spectra (except for 39.7 + 1.5 and 127.8 + 0.0) have been slightly adjusted to order to match the two LRS bands in the overlapping wavelength region. The strengths of the silicate absorption feature derived from fitting of the continuum for these objects are given in Table 3.

The seven LRS spectra in Figure 5 are arranged in increasing kinematic distances from top to bottom, as in Figure 3 of Gehrz *et al.* The linear relationship of τ and distance is not substantiated. We must therefore conclude that there is no empirical evidence for interstellar extinction playing a major role in the formation of the silicate feature in OH/IR stars.

TABLE 3

STRENGTHS OF THE SILICATE FEATURE FOR SEVEN OH/IR STARS IN THE GALACTIC PLANE

Object	*IRAS* Name	s
26.2−0.6.....	18385−0617	10.01
26.4−1.9.....	18437−0643	3.24
35.6−0.3.....	18549+0208	6.12
39.7+1.5.....	18560+0638	8.21
39.9+0.0.....	19017+0608	6.36
42.3−0.2.....	19065+0832	5.79[a]
127.8+0.0.....	01304+6211	14.31

[a] The value for s may have been underestimated because of problems in matching the two LRS bands.

VI. ORIGIN OF THE 10 MICRON ABSORPTION FEATURE

Since our sample of oxygen-rich AGB stars is the result of a sensitivity-limited all-sky survey, we can draw certain statistical conclusions on the nature of AGB stars which were not possible in the past because of the inherent biases of previous infrared or radio surveys of OH/IR stars. The population ratio of the emisssion to absorption objects suggests that (1) not all emission objects evolve into absorption objects, and/or (2) the duration of the absorption phase is much shorter than the emission phase. Since stars with higher mass evolve further up the AGB and develop higher mass-loss rates and therefore thicker circumstellar envelopes, the absorption objects as a group may have higher main-sequence masses than the emission objects which deplete their hydrogen envelopes before the silicate feature goes into self-absorption. The relative size of the two groups may therefore be the result of the initial mass function. If mass-loss rates $>10^{-5}\ M_\odot\ \mathrm{yr}^{-1}$ are required to lead to silicate self-absorption, then the duration of this phase is also likely to be shorter according to AGB evolutionary models (Kwok 1983).

The population difference between the emission and absorption objects is also evident in their respective galactic distributions. The galactic distributions of 323 of the LRSC 20–29 objects with good photometry and all the LRSC 30–39, 70–79 objects are plotted in Figures 6*a* and 6*b*, respectively. The emission objects cover a wide latitude range and must be relatively nearby (<1 kpc) objects whereas the absorption objects are located within a few degrees of the plane. This implies that either (1) the absorption sources are statistically farther away (and therefore intrinsically brighter) or (2) their galactic distribution reflects the distribution of their more-massive progenitors. Since (1) would be a consequence of (2) if we take into consideration that more luminous AGB stars are likely to have descended from higher mass progenitors, we can conclude that only stars with main-sequence mass higher than a certain value (e.g., 3 $M_\odot$) develop self-absorption silicate features.

VII. THE ROLE OF INTERSTELLAR EXTINCTION

The galactic distributions shown in Figure 6 suggest that nearly all of the absorption objects are in the plane. This, however, does *not* imply that the 10 μm feature is created by interstellar extinction for the color of these objects is simply too red to be caused by extinction alone (§ III).

We may also note that carbon stars are intrinsically bright objects and can be seen at large distances. The fact that no carbon star (either identified in the visible or by the presence of the SiC feature) shows the silicate feature in absorption is an indication of the limited importance of interstellar extinction.

The major limitation of the present study may be that the sensitivity limit of the LRS restricts our sample to only relatively nearby objects and therefore minimizes the contribution from interstellar extinction. While we have shown that the silicate feature is unlikely to be of interstellar origin, we have not demonstrated that interstellar extinction plays no part in the formation of the absorption feature. In fact, a number of sources in the *IRAS Point Source Catalog* identified by Kwok, Hrivnak, and Boreiko (1987) at the Canada-France-Hawaii

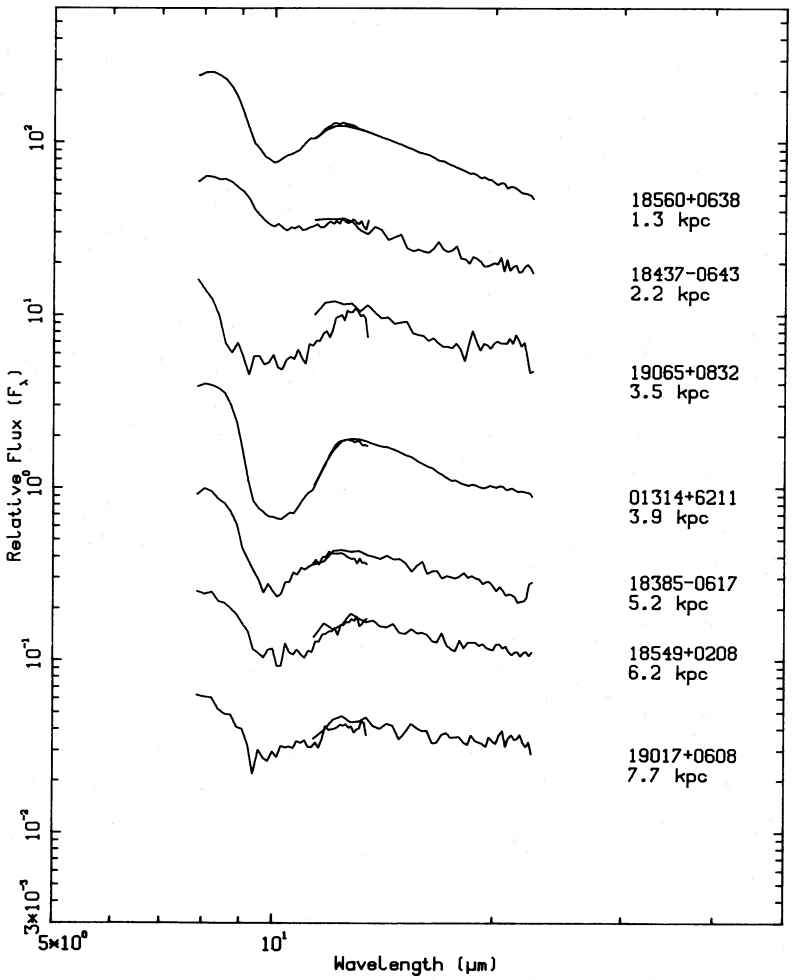

FIG. 5.—The LRS spectra of seven OH/IR stars in Gehrz *et al.* (1985) plotted in order of increasing near kinematic distance

Telescope show deeper absorption features than those in the LRSC, and the excess could be the result of interstellar extinction. In order to quantitatively evaluate the effects of interstellar contribution, a more comprehensive study of cool and faint infrared sources is required. Assuming that the sample of faint sources and the present LRS sample are intrinsically the same but differ only in distance, the depths of the 10 μm feature in the two samples can be compared. Any differences can then be attributed to interstellar extinction.

VIII. CONCLUSION

We have studied a sample of 467 oxygen-rich stars in the *IRAS* LRSC which show the 10 μm dust feature in either emission or absorption. The relative population and Galactic distribution of emission and absorption objects suggest that the absorption objects originate from a higher mass main-sequence population and not all AGB stars go through the 10 μm self-absorption phase.

Color temperatures for stars in this sample are determined from the four *IRAS* photometric fluxes, and from these data we find no evidence of silicate dust absorption against the photospheric ($T > 3000$ K) continuum. All sources with the 10 μm feature in absorption have color temperatures below 660 K, while in the entire sample (with three exceptions) the highest temperature is ~1700 K, which should be the upper limit to the dust condensation temperature. The low color temperature of the absorption objects and the decreasing trend in the color temperature of the continuum as the strength of the dust feature increases, are best interpreted by a mostly circumstellar origin of the 10 μm dust feature.

An examination of the LRS spectra of seven of the 11 sources used by Gehrz *et al.* (1985) to derive the optical depth–distance relationship has failed to support that empirical relationship. There is no evidence for significant interstellar contribution to the strength of the silicate feature for the AGB stars in the LRSC.

It is likely that interstellar absorption will increase the strength of the silicate absorption feature for more distant sources. The exact degree of contribution of interstellar extinction to the strength of the 10 μm feature can only be determined from a larger sample of fainter sources. The present study will constitute as a comparison sample for such a future study.

The *IRAS* Low Resolution Spectra Catalog is provided on magnetic tape in machine-readable form by the World Data Center in Greenbelt, Maryland. Mr. C. T. Haglund assisted in

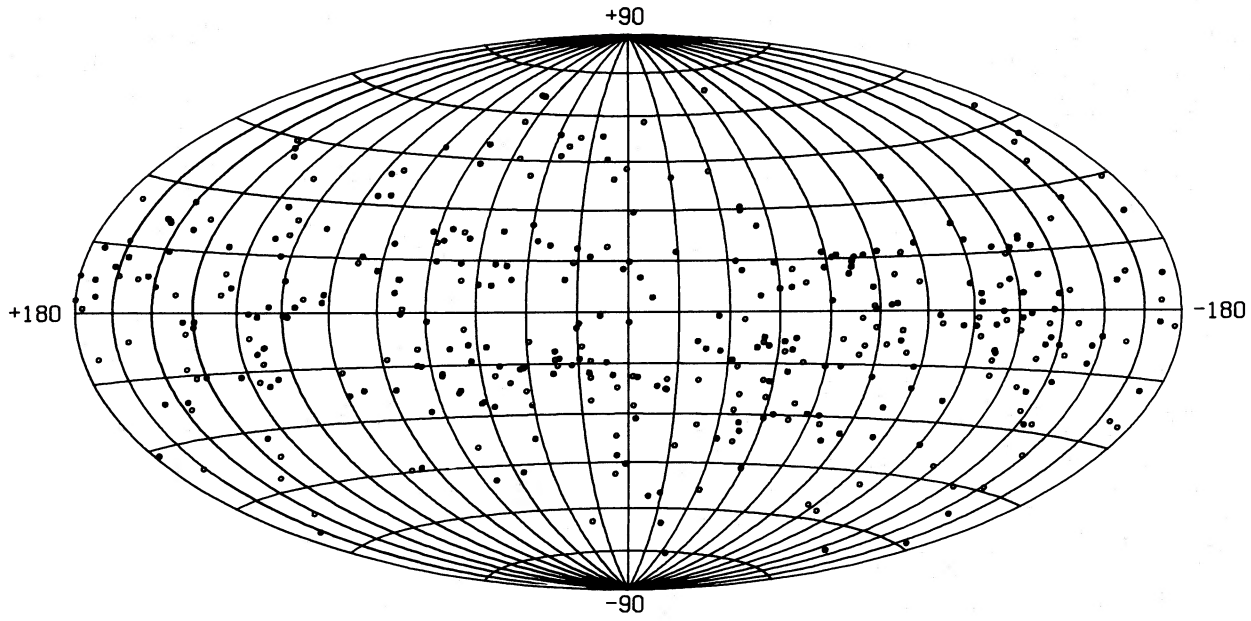

FIG. 6a

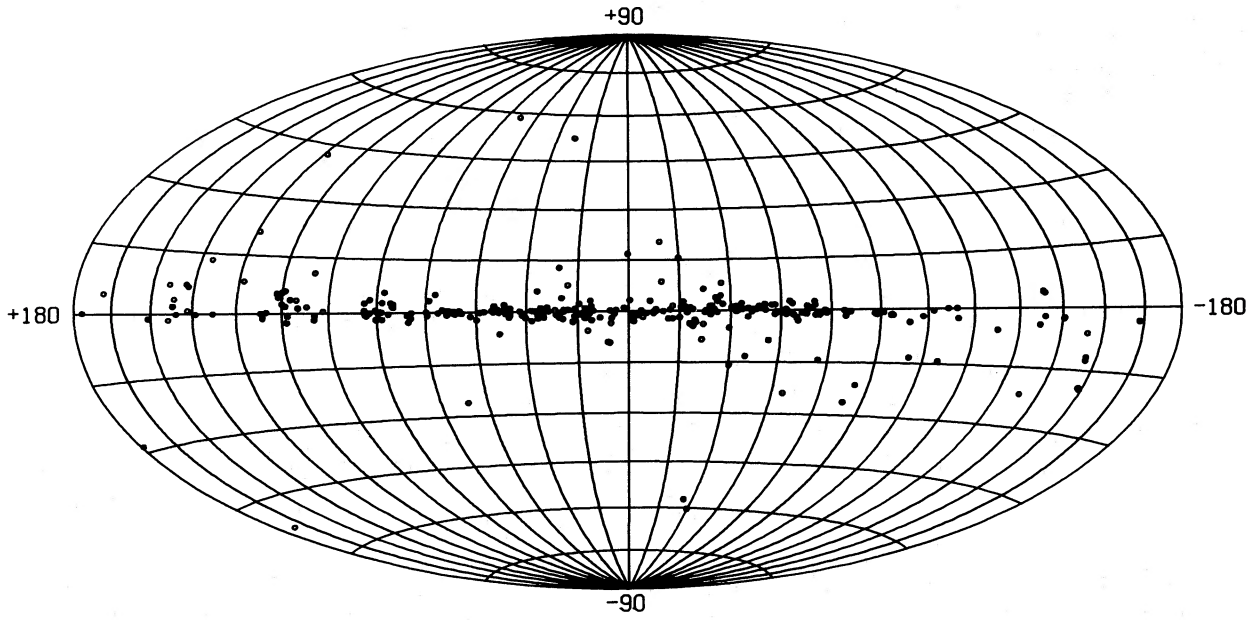

FIG. 6b

FIG. 6.—(*a*) The Galactic distribution of objects with the 10 μm feature in emission. The LRSC 20–24 objects are shown as open circles and LRSC 25–29 objects as filled circles. (*b*) The Galactic distribution of objects with the 10 μm feature in absorption. The LRSC 30–39 objects are shown as open circles and LRSC 70–79 as filled circles.

the development of software for the analysis of the LRS spectra, and Miss J. S. Chan assisted in the calculation of color temperatures. The *IRAS* data reduction facility is supported by a grant from The University of Calgary. S. K. acknowledges the award of an operating grant from the Natural Sciences and Engineering Research Council of Canada.

REFERENCES

Evans, N. J. II, and Beckwith, S. 1977, *Ap. J.*, **217**, 729.
Gehrz, R. D., Kleinmann, S. G., Mason, S., Hackwell, J. A., and Grasdalen, G. L. 1985, *Ap. J.*, **290**, 296.
Herman, J., Isaacman, R., Sargent, A., and Habing, H. J. 1984, *Astr. Ap.*, **139**, 171.
IRAS Catalogs and Atlases, Explanatory Supplement. 1985, ed. C. A. Beichman, G. Neugebauer, H. J. Habing, P. E. Clegg, and T. J. Chester (Washington, D.C.: U.S. Government Printing Office).
Kwok, S. 1983, in *IAU Symposium 103, Planetary Nebulae*, ed. D. R. Flower (Dordrecht: Reidel), p. 293.

Kwok, S., Hrivnak, B. J., and Boreiko, R. T. 1987, in preparation.
Merrill, K. M., and Stein, W. A. 1976*a*, *Pub. A.S.P.*, **88**, 285.
———. 1976*b*, *Pub. A.S.P.*, **88**, 294.
———. 1976*c*, *Pub. A.S.P.*, **88**, 874.
Volk, K., and Kwok, S. 1987, in *Late Stages of Stellar Evolution*, ed. S. Kwok and S. R. Pottasch (Dordrecht: Reidel), p. 305.
Werner, M. W., Beckwith, S., Gatley, I., Sellgrem, K., Berriman, G., and Whiting, D. L. 1980, *Ap. J.*, **239**, 540.
Woolf, N. J., and Ney, E. P. 1969, *Ap. J.* (*Letters*), **155**, L181.

S. Kwok and K. Volk: Department of Physics, The University of Calgary, Calgary, Alberta, Canada T2N 1N4